Chemistry Africa (2023) 6:747–756
https://doi.org/10.1007/s42250-022-00482-6

ORIGINAL ARTICLE

Real heavy crude oil desulfurization onto nanoporous activated carbon implementing batch adsorption process: equilibrium, kinetics, and thermodynamic studies

Yusra A. Abd Al-Khodor[1] · Talib M. Albayati[1]

Received: 12 August 2022 / Accepted: 12 September 2022 / Published online: 25 September 2022

Abstract
In the current study, the desulfurization process was adopted for sulfur content removal from the real heavy crude oil (HCO) containing 2.5 wt.%. The desulfurization process of HCO was carried out by implementing a batch adsorption desulfurization process with AC as an adsorbent. The sorbent activated carbon (AC) was characterized. The operating conditions, such as the AC dose, temperature, and contact time were examined. It was found that 0.8 gm AC, 50 °C, and 90 min were the optimal operating parameters. The Langmuir, Freundlich, and Temkin isotherm model types have all been employed. The adsorption isotherm of Temkin models with a determination coefficient ($R^2 = 0.99$) provided the best representation of the data. The kinetics models were investigated such as; pseudo-first and second-order in addition to the Intra-Particle diffusion. The adsorption process was observed to obey a pseudo-first-order adsorption kinetic model under a determination coefficient R^2 of 0.95. The Gibbs Free Energy (ΔG^o), Entropy (ΔS^o), and Enthalpy (ΔH^o) were calculated. According to the results, sulfur adsorption is endothermic, spontaneous, and enhances the random pattern of sulfur molecules onto the surface of adsorbent. The desulfurization efficiency of the processed crude oil was 28%, with the sulfur content dropping from 2.5 to 1.8%.

Keywords Adsorption desulfurization · Activated carbon adsorbent · Real heavy crude oil · Sulfur removal · Environmental pollutants · Batch adsorption · Desulfurization · Environmental treatments · Batch adsorption desulfurization

1 Introduction

Techniques for purifying crude oil can eliminate pollutants and impurities, particularly sulfur-harmful byproducts that are manageable by traditional approaches implementing a combination of chemical, physical, and biological processes. Several refineries worldwide deal with a range of strategies to minimize the sulfur content of crude oil [1–3]. For a variety of reasons, desulfurization by adsorption is characterized as being amongst the most significant desulfurization procedures, notably the need for moderate operating conditions, effective desulfurization, and strong selectivity for thiophene molecules [4, 5]. It is the technique most frequently applied to obtain ultra-clean hydrocarbons [6]. Adsorption is a mass transfer phenomenon that involves binding free-radical molecules to a surface as a result of forces within molecules. It is extensively utilized to eliminate trace pollutants, such as removing trace amounts of aromatics from aliphatics [7]. It can be used effectively with low sorbate level separation procedures, and as a result, it has the potential to be used in separation processes that remove refractory sulfur compounds from transportation fuels [8]. Numerous solids, primarily, can be categorized into two groups: natural and artificial, are served as adsorbents to clear out impurities from liquids. Natural adsorbents usually involve charcoal, zeolites, clay minerals, and clays, whereas artificial adsorbents include activated carbon, molecular sieves, silica gel, activated alumina, and others [9]. In 2005, Yu et al. [10] examined industrial diesel desulfurization for dibenzothiophene (DBT) via activated carbon. In the existence of formic acid and activated carbon, a diesel fuel containing 800 ppm sulfur and H_2O_2 was investigated. The sulfur in diesel oil was reduced, with 82% of the oil being recovered. Jabbar (2013) [11] researched the influence of the oxidizing agents H_2O_2, AC, and formic acid on the crude oil desulfurization. A 32.3% efficiency was achieved throughout the crude oil

✉ Talib M. Albayati
Talib.M.Naieff@uotechnology.edu.iq

[1] Department of Chemical Engineering, University of Technology, 52 Alsinaa St., PO Box 35010, Baghdad, Iraq

desulfurization process by reducing the sulfur concentration from 3.9 wt.% to 2.622 wt.%. In 2015, Al Zubaidi et al. [12] examined the adsorption of sulfur components from normal diesel oil onto granular activated charcoal (GAC). The data showed that, in relation to the initial specimen, the sulfur concentration had dropped by 20.9%. Ibrahim 2015[13], focused on using AC to desulfurize industrial diesel fuel. The efficiency of desulfurization was 57% as the residual sulfur content in diesel fuel dropped from 580 to 247 ppm.

As indicated above, very little desulfurization studies of actual heavy crude oil employing batch adsorption process were found in the literature, because of difficult to deal with, high sulfur content, high boiling points, low API and high viscosity due to organic sulfur compounds.

In this work, a technique of batch adsorption desulfurization was explored to minimize the sulfur content of real heavy crude oil from the Halfaya Oil Field in southern Iraq, which had a sulfur level of 2.5 wt%. Activated carbon (AC) was used in this approach as an effective adsorbent. The influence of several operating conditions was explored, such as; the AC dose, time of contact, and temperature. The sulfur removal process was outright with three models of isotherms. Three kinetics approaches were used to evaluate the sulfur component kinetics on activated carbon. Thermodynamic properties such as; Gibbs free energy, entropy (ΔS^o), and enthalpy (ΔH^o) were studied. The experimental technique was used to accomplish the desulfurization pathway in an auto cleave batch reactor.

2 Materials and methods

2.1 Chemicals

Crude oil from the oil field of Al-Halfaya in southern Iraq was used for testing. The chemicals that were used include Formic acid (CH_2O_2, 95% purity), Hydrogen peroxide (H_2O_2, 93% purity), and distilled water (H_2O), and Activated carbon (AC) purchased from regional stores. The chemicals, which were all obtained from Sigma Aldrich, were used in their original form.

2.2 Characterization of AC

The patterns exhibited by x-ray powder diffraction on the AC sample were employed to show the crystalline structure and were acquired by implementing a diffract meter with X-rays (Originating from Japan, type: Shimadzu-6000) by a radiation of Cu Kα (λ 1.154 A), utilizing a 2 (deg/min) scan rate and 2θ in the range of 0°–10°. The D-spacing and unit cell parameters were determined by applying the formulas $n\lambda = 2d\sin\theta$ and $a_o = 2d100/\sqrt{3}$. The AC chemical compositions were analyzed by using a scanning electron microscope (SEM) examination using backscattered electron (BSE) with secondary electron (SE) at a 20 kV voltage acceleration. The FTIR (Fourier transform infrared spectroscopy), which is utilized with AC technologies, spectra show a broad range of spectrum groups. The frequency range that demonstrates the expanded vibrations could also be associated with chemical bonding. The standard method to prepare solid sample for FTIR spectrometer is to use KBr. About 2 mg of sample and 200 mg KBr are dried and ground. The particle size should be unified and less than two micrometers. Then, the mixture is squeezed to form transparent pellets which can be measured directly. The measurements of the samples, such as; the (BET) surface area, average particle diameter, pore size, pore volumes, and real density, were performed. A furnace was used to dry the AC at 110 °C for 4 h ahead of the measurement to exclude all moisture that may have been retained.

2.3 Method of analysis

The concentration of sulfur in samples of unprocessed and processed crude oil was measured using X-ray analysis in conformity with (ASTM D-4294) by Horiba Ltd., Japan. These kinds of tools are fitted with the membrane spectra that typically serve as a support for the extremely thin layers of a frame mount material. The percentage of sulfur components that have been removed is determined by using the proportion of removed (or eliminated) sulfur compounds to their content within crude oil as provided in the Eq. (1) [14–16]:

$$\text{Removal}\,\% = \frac{C_i - C_e}{C_i} \times 100\% \tag{1}$$

where $\boldsymbol{C_e}$ is the equilibrium adsorbate concentration (mg/L) and $\boldsymbol{C_i}$ is the initial concentration (mg/L).

2.4 Desulfurization experiments

The experiments of batch adsorption were achieved for actual HCO desulfurization in a 250 ml flask with activated carbon. The used average particle size was 0.8 mm AC, and the moisture content was first removed by drying the material for 4 h at 110 °C within a furnace. In the first step of the procedure, 50 ml of processed oil was mixed with 3 mL H_2O_2, 4 mL of formic acid, and 5 ml distilled water. Accordingly, the abovementioned solution is thus supplied with 0.2 to 1 g of activated carbon. The flask was set on a hot plate magnetic stirrer that was submerged in water to adjust the temperature between 20 and 50 °C, and it was rotated at 500 rpm for 15 to 120 min to reach the equilibrium state. Then, the solution was left time to cool at ambient temperature. The mixture of reactions was then put into a centrifuge to separate the particles of AC from the reaction mixture,

wherein the sulfur concentration was calculated. The experiments were performed in a laboratory that belongs to the Chemical Engineering Department. The experiments were repeated three times; the average data was shown to have an error of less than ± 3%. The ranges of operating parameters, such as the AC dose (0.2–1.0 gm), temperature (30–50 °C), and contact time (15–120 min), Formic acid (4 mL), and Hydrogen peroxide (3 mL) were investigated.

A total sulfur analyzer equipment was used to measure the total sulfur content concentration, which showed an error of less than ± 5%. The results of the treatment were evaluated using X-ray fluorescence, which is identical to (ASTM D-4294) and made in Japan by Horbia Ltd.

2.5 Adsorption isotherm model

2.5.1 Langmuir isotherm

Langmuir isotherm governs monolayer adsorption that occurs on an adsorbent surface when there are only a limited number of adsorbent sites available. The isotherm is based on the supposition that adsorbate transmigration does not happen in the plane of the surface, and the surface maintains similar adsorption energies. In addition, there are no lateral interactions between the molecules of the sorbent [17].

Equation (2) provides the Langmuir linear model.

$$\frac{C_e}{q_e} = \frac{C_e}{q_{max}} + \frac{1}{bq_{max}} \tag{2}$$

where q_{max}: Langmuir constant relating to adsorption capacity (mg/g), b: constant indicates the adsorption energy (L/mg). The q_{max} and b constants are calculated from Eq. (3) by the linear plot slope of Ce/qe versus Ce.

Furthermore, the parameter R_L for dimensionless equilibrium refers to the isotherm is unfavorable, favorable, and linear, or irreversible whenever the value of $R_L < 1$, $R_L > 1$, $R_L = 1$, and $R_L = 0$, respectively. As shown in Eq. (3):

$$R_L = \frac{1}{1 + bC_i} \tag{3}$$

In this equation, *Ci* represents the initial concentration of sulfur in (mg/L).

2.5.2 Freundlich isotherm

It is clarifying the multilayer adsorption process, which is heterogeneous (not homogeneous) [18], with a heat and adsorption affinity distribution which is not homogeneous. It is assumed that stronger binding sites are first occupied and as the site occupancy increases, the energy of adsorption decreases [19]. The linear form is expressed by Eq. (4):

$$\ln q_e = \ln K_f + \frac{1}{n}\ln Ce \tag{4}$$

where q_e is how many processes were performed on the absorbent's surface (mg/g), the constant K_f intends to describe the sorbent's adsorption capability (mg/g). Adsorption intensity based on the n value, good characteristics, moderate adsorption, and poor adsorption is observed when $n = 2–10$, $n = 1–2$, and $n < 1$ respectively [20].

2.5.3 Temkin isotherm

Temkin isotherm suggests that upon complete coverage of all adsorbate molecules, the heat of adsorption across the layer is linearly decreased due to the interactions between the adsorbate and adsorbent as well as the notion that a uniform energy distribution makes the absorption obvious [20, 21]. The above model is different from the Langmuir model, which combines a special factor for the sorbent interactions and sorbent species [22, 23]. The Temkin linearized form isotherm model is expressed as:

$$q_e = B\ln K_t + B\ln Ce \tag{5}$$

where K_t is the binding constant of equilibrium (L/g) equivalent to the maximal binding energy, B is the Temkin constant (J/kJ), and it can be given by the Eq. (6):

$$B = \frac{RT}{b_t} \tag{6}$$

Where b_t is the adsorption heat (kJ/mol), R is the universal gas constant (8.314 J/mol K), and T is the temperature (K).

2.6 Adsorption kinetics models

2.6.1 First-order kinetic

The kinetic parameters were correlated to pseudo-first-order. Equation (7) shows the linear profile [24]:

$$\log(q_e - q_t) = \log q_e - \left(\frac{K_1}{2.303}t\right) \tag{7}$$

where q_e is the sulfur adsorbed amount at equilibrium (mg/g). q_t is the sulfur absorbed amount (mg/g) at the time (t). K_1: The equilibrium rate constant of the pseudo-first model, (min^{-1}). The K_1, q_e, and the values of R^2 are taken out from the intercept and slope of the linear equation graph.

2.6.2 Second-order kinetic

Equation Eq. (8) represents the kinetic interaction of the pseudo-second-order [25]

$$\frac{t}{q_t} = \frac{1}{K_2 q_e^2} + \frac{1}{q_e} t \tag{8}$$

Since the rate constant of the pseudo-second-order model is K_2, measured in (g/mg min) which is calculated by plotting t/q_t versus t.

2.6.3 Intra-particle diffusion

The model of intra-particle diffusion is represented by Weber's intraparticle according to the Eq. (9) [26, 27]:

$$q_t = K_{id} t^{0.5} + C \tag{9}$$

where K_P is the rate constant of intra-particle diffusion (mg/g $min^{0.5}$), and I; is the constant of intra-particle diffusion.

where K_{id} is the coefficient of intraparticle diffusion (mg/g$(min)^{0.5}$) and C is the intra-particle diffusion constant, which reveals the boundary layer thickness (boundary resistance).

2.7 Adsorption thermodynamics

Thermodynamic variables were estimated to evaluate the entropy change (ΔS^o), enthalpy change (ΔH^o), and free energy change (ΔG^o) applying the Gibbs free energy change [28]:

$$\Delta G^\circ = -RT \ln K_C \tag{10}$$

where R is the universal gas constant (8.314 J mol^{-1} K^{-1}) and T is the temperature in K. The apparent adsorption equilibrium constant (K_C) is expressed in the form:

$$K_C = \frac{q_e}{C_e} \tag{11}$$

$\Delta G^o = \Delta H^o - T\,\Delta S^o$ (12)

Equating the Eqs. 10 and 12 resulted in the Van't Hoff equation:

$$\ln K_C = \frac{\Delta S^\circ}{R} - \frac{\Delta H^\circ}{RT} \tag{13}$$

where ΔH^o and ΔS^o (J/mol) are obtained from the slope and intercept of the Van't Hoff equation for the relationship between $ln\ K_c$ and 1/T Eq. (13).

3 Results and Discussion

3.1 Characterization of AC

The actual HCO analysis sample was employed in this study and examined at the Laboratory of the Halfaya Oil Field, as explained in the previous work [14]. The X-ray pattern of the solid AC is shown in Fig. 1.

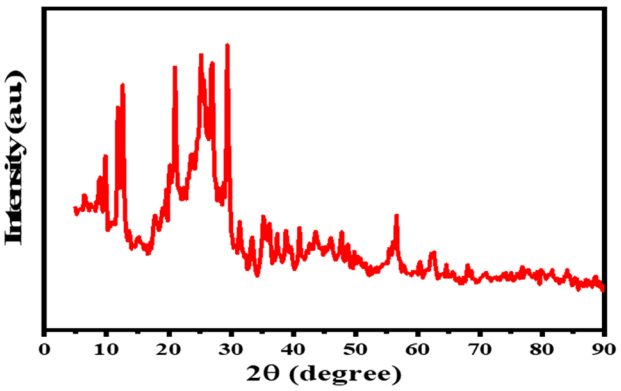

Fig. 1 XRD pattern of activated carbon

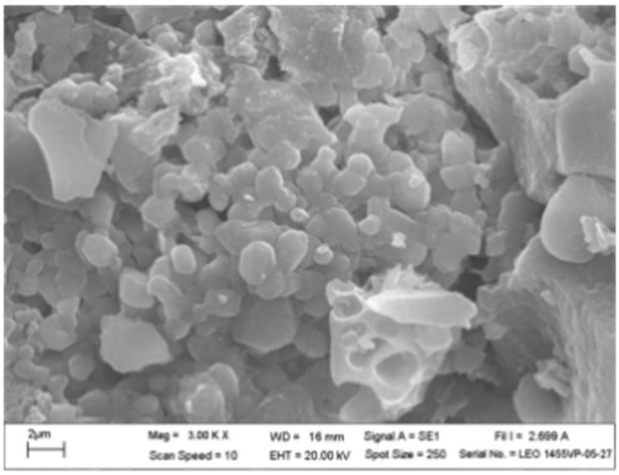

Fig. 2 Surface structure for activated carbon

XRD is the most important method to show the nanoparticle size and crystalline and amorphous materials. Researchers have worked on X-Ray diffraction analysis of activated carbons, concluded that predominantly amorphous solid having large internal surface area and pore volume [29]. The diffraction angle (2θ) of the 002 peak of crystalline graphite is known to be 12°, but the 002 peak in this figure was located near 21°. It was reported that XRD patterns for each of the activated carbon indicated a shape of typical amorphous carbon and showed broad asymmetric peaks corresponding to $2\theta = 25°$ and $2\theta = 56°$. However, broad peaks in the XRD pattern represent the amorphous structure of the activated carbon, while sharp peaks reveal the crystal structure [30]. This is an advantageous adsorption feature of activated carbon. The AC morphology analysis was achieved by implementing SEM equipment (Type: VEGA 3 LM, Origin: Germany) to evaluate porosity and the texture of the specimen surface. Figure 2 illustrates the Surface formation of the AC. Scoping the surface of

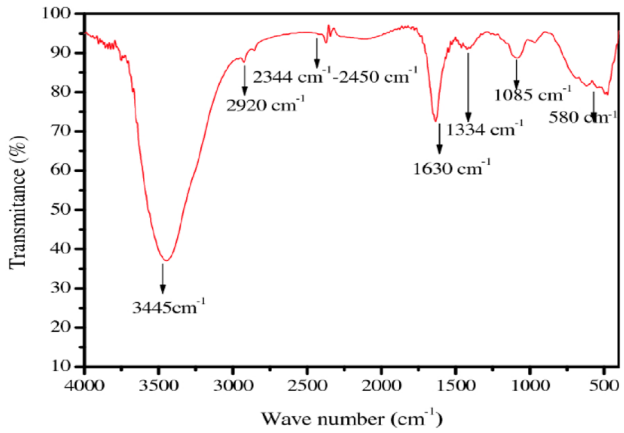

Fig. 3 FTIR spectrum of activated carbon

the AC more precisely revealed the presence of mesoporous channels that were identical in size and spherical in shape, puffy or swollen forms as well as normal surfaces, approximately around (500 nm in diameter). Such puffy structures are convenient for sulfur components adsorption.

The spectrum of FTIR analyses of the activated carbon can be seen in Fig. 3. It is possible to view the range of various frequency groupings as well as the band which appears at 3700 cm^{-1} was attributed to the stretching vibrations available in the bonds between N and H. Furthermore, around 3100 and 3500 cm^{-1}, O–H bond stretching modes can be observed. The bending vibration of CH_2 is compatible with the absorption bands at 2920 cm^{-1}. The broad peak for N=O is between 1300 and 1500 cm^{-1}, while the bending peaks for C=O are at 1500 cm^{-1}. The carboxylate and ether molecules are stretched by the C–O bands at 1200 cm^{-1}. These functional groups are necessary for the adsorption of contaminants containing sulfur. The analysis of FTIR spectra indicates the identical nature of emerging intermolecular interactions for H-aggregates and hydrates. Intermolecular hydrogen bonds and π–π interaction of sulfur compound aromatic rings were observed during self-association [31].

The physical properties of AC according to ISO-9277–2010 are as follow: BET surface area (m^2/g) = 519, total pore volume (cm^3/g) = 0.36, average particle diameter (mm) = 0.8, pore size (nm) = 0.18–1.8 and real density (g/cm^3) according to ASTM D 5550 = 2.84. Surface area, real density, and porosity measurements were performed at the Institute for Petroleum Research and Development in the catalyst laboratory.

3.2 Batch adsorption desulfurization process

3.2.1 Effect of dose and contact time

The amount of sulfur eliminated rises steadily in proportional measure to the increase in the dose of sorbent from 0.2 to 0.8 gm, thus the efficiency of removal rose from 3.6 to 23.2%, while the removal is almost constant when the dose of sorbent is increased from 0.8 to 1 gm. The rise in sulfur element adsorption with boosting adsorbent dose might just be attributed to the increased surface area availability and adsorption sites for the process of adsorption of sulfuric elements from heavy crude oil [32]. Besides, the rise in adsorption with a high dose of sorbent is also primarily attributable to the fact that AC catalyzes the decomposition of hydrogen peroxide to generate hydroxyl radicals through a range of free radical reactions, which are severe as strong oxidizing agents. According to the conception, sulfur compounds oxidize to form $SO4^{-2}$ and are then eliminated into the aqueous phase [21], as elucidated in Fig. 4.

Formic acid and H_2O_2 were simultaneously added into the reaction, and the oxidative reaction will happen, so the sulfur compounds which possess higher electron density will be converted to sulfone. One more thing, H_2O will be formed after the oxidative reaction. H_2O possesses a higher polarity, which will occupy the active site of AC material. Increasing contact times contributed to a greater lowering of sulfur particles. According to Fig. 4, after 90 min, up to 23% of the material had been removed, as contrasted to 1.6% after 15 min. Additionally, the interaction of both the phases (crude oil contains sulfur molecules and sorbents) is more effective as blending time increases, especially at 500 rpm speed. This figure clearly shows that after 1.5 h, there is no considerable variation in the desulfurization efficiency owing to the adsorption of sulfones and alkyl-substituted

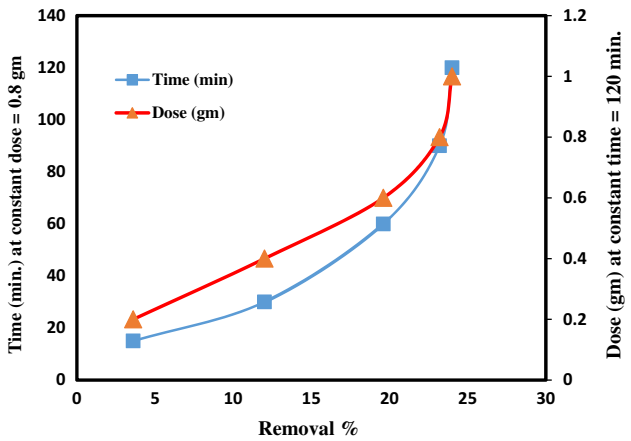

Fig. 4 Removal of sulphur content against time and sorbent dose at blending speed 500 rpm and 30 °C

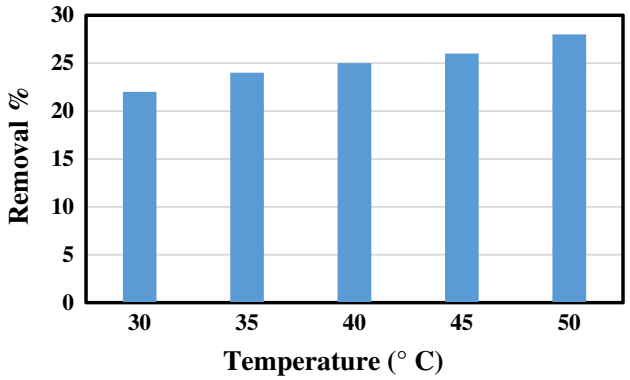

Fig. 5 Sulfur content versus Temperature at 500 rpm mixing speed, 90 min and 0.8 gm sorbent dose

sulfoxides generated throughout oxidation on the surface of the AC, consequently restricting the adsorption process. The achieved results mostly match with the observations of [33].

3.2.2 Effect of temperature

The elimination of sulfur particles improves from 22.4 to 28.3% as the range of temperatures is elevated from 30 to 50 °C, as demonstrated in **Fig. 5**.

The relatively high temperature (50 °C) enhances the capacity of sulfur components to be adsorbed from crude oil, also because of its potential impact on minimizing the viscosity of relatively high viscosity crude oil, thus facilitating better sulfur compound diffusion and hence improving the oxidation [34]. According to numerous studies, increasing the temperature up to 50 °C (from 30 °C) enhances the removal of sulfur-containing components. However, once the temperature passed (50 °C), it had the reverse effect, primarily due to the formation of resins and asphaltenes as well as the degradation of the oxidant utilized. Furthermore, the increasing temperature beyond (50 °C) leads to change the heavy crude oil performance [35].

3.3 Adsorption isotherm model

The data of equilibrium adsorption were applied to Langmuir, Freundlich, and Temkin isotherms. The equilibrium capacities, rate constants, and related correlation coefficients are demonstrated in Figs. 6a–c for each isotherm. The Temkin isotherm model had a better correlation coefficient ($R^2 = 0.99$) and better agreement with the experimental data. As seen in Fig. 6c, Kt (L/mg) = $3.098*10^{-5}$ and b_t (KJ/mol) = − 0.003 were obtained by using the intercept and slope of the linear plot of qe vs. ln Ce. The negative value of b_t reveals an endothermic condition

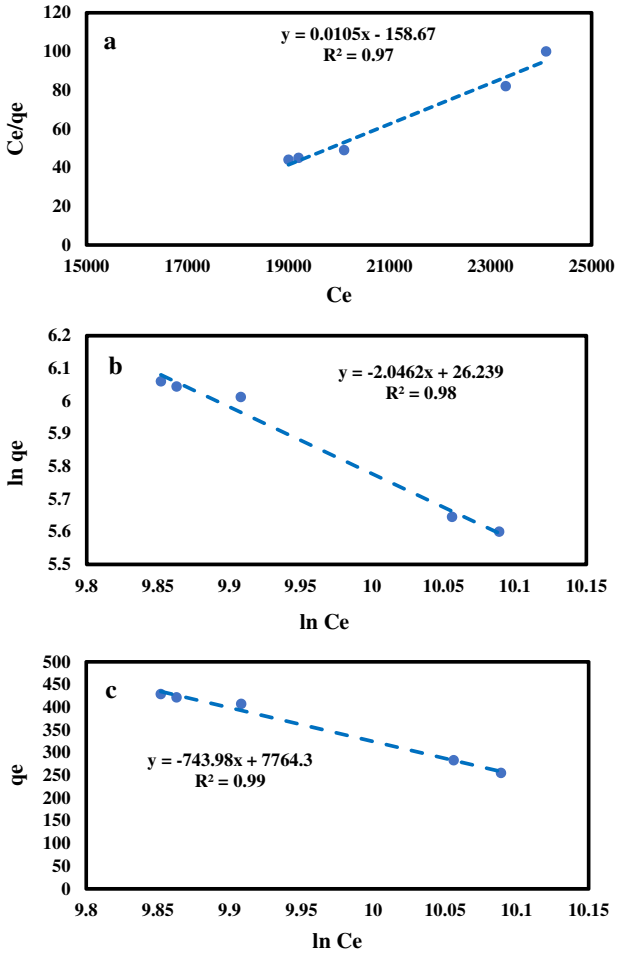

Fig. 6 **a** Langmuir, **b** Freundlich and **c** Temkin isotherms

throughout the process [36]. The value of R^2 (0.99) suggests that the Temkin model for explaining the adsorption of sulfur components on the AC adsorbent appears to be the most appropriate model when compared to the Freundlich and Langmuir models of isotherm. Moreover, by analyzing the calculated experimental results, the Langmuir isotherm and the R_L value is 0.38 more than 0 but below 1 referring that the Langmuir isotherm was also favorable, the capacity of maximum monolayer coverage $q_{max} = 87$ mg/g with correlation coefficient $R^2 = 0.98$. The measurements of b (L/mg) = $6.5*10^{-5}$ and $q_{max} = 87$ mg/g were acquired from the Eq. (2) by the intercepts and slope of the graph of (C_{eq}/q_e) against (C_{eq}) are given in Fig. 6a. The Freundlich isotherm graph is displayed in Fig. 6b. $1/n = 0.41$ and K_f (mg/g) = $3.32*10^{13}$can be determined by the slope and intercept of the Ln qe versus Ln Ce plot. The relatively high values of ($R^2 = 0.97$) demonstrate that the experimental data matches the Freundlich isotherms model [37].

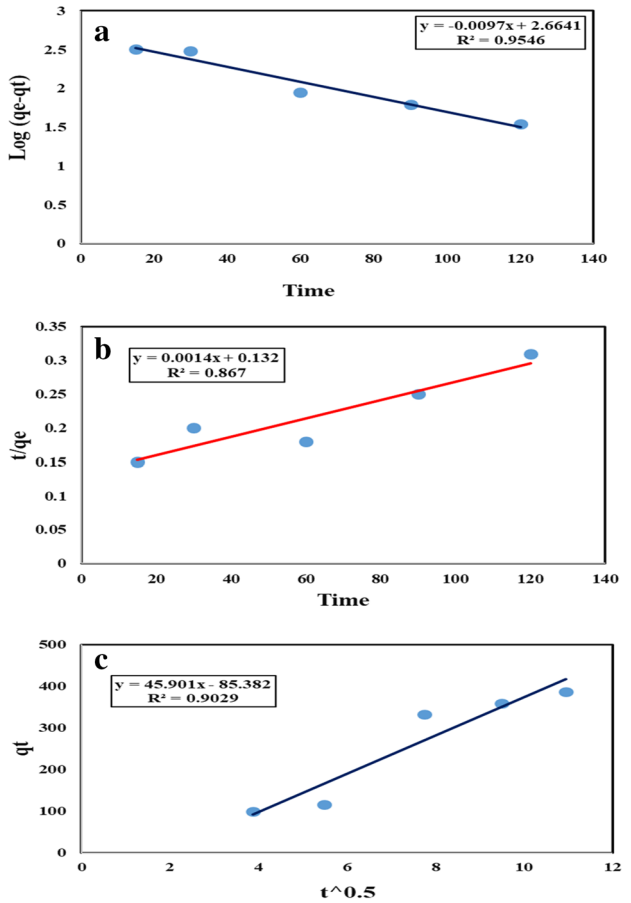

Fig. 7 **a** First order, **b** Second order and **c** Intra-Particle diffusion kinetics

Table 1 Intraparticle Diffusion Parameters for desulfurization by the Weber-Morris Model using activated carbon

Pseudo-first order	q_e (mg/g)	K_1 (min^{-1})	R^2
	457	0.0223	0.95
Pseudo-second order	q_e (mg/g)	K_2 (gmg^1min^{-1})	R^2
	714.28	1.48*10–5	0.87
Intra-particle diffusion	C	K_{id} ($mg/g.min^{0.5}$(	R^2
	85.38	45.901	0.90

3.4 Kinetics of adsorption

The rate at which sulfur components are adsorbed from heavy crude oil was discussed by applying various kinetic models of pseudo-first-order, second-order, and intraparticle models. The kinetic result was matched to a pseudo-first-order adsorption model more than the pseudo-second-order, in which the regression coefficient value (R^2) was 0.95 as shown in Fig. 7a and Table 1 [38, 39].

Table 2 Thermodynamic parameters for the desulfurization using activated carbon

Temperature (K°)	ΔH° (kJ/mol)	ΔG° (J/mol)	ΔS° (J/mol.K)
303	3.255	– 1939.73	17.098
308		– 2022.96	
313		– 2040.50	
318		– 2194.39	
323		– 2282.60	

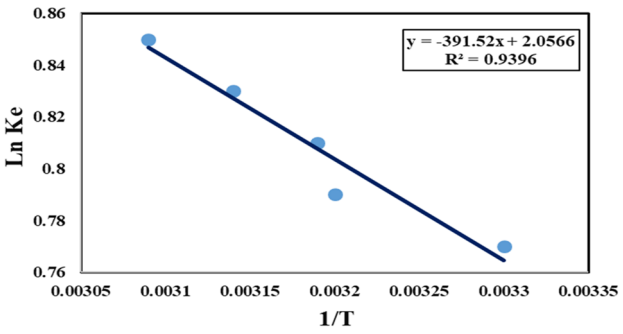

Fig. 8 Thermodynamic for the desulfurization of activated carbon

In Fig. 7b, the relationship between (t/q_t) and the required time was displayed to acquire K_2 and q_e for second-order. Table 1 summarizes calculated values for second-order kinetics. The value of R^2 was equal to 0.87, which is less than pseudo-first-order. Consequently, the q_e acquired theoretical values were approved with the experimental values. The R^2 and kinetic variables values were correlated with different models and summarized in Table 1. Moreover, the values proved the appropriateness of the first-order model for sulfur adsorption from heavy crude oil onto AC. Furthermore, a model of intraparticle was used to get the adsorption process rate-limiting step [40]. Regression lines are manifested in Fig. 7.c, not passing through the origin (not all points fall within the domain of the regression line). Thus, this demonstrates that there are other mechanisms besides intra-particle diffusion that determine the rate, revealing the potential of additional processes. Considering intra-particle diffusion, the constants are depicted in Table 1.

3.5 Adsorption Thermodynamics

The influence of thermodynamic parameters on the adsorption rate of sulfur components from heavy crude oil is presented in Table 2 and Fig. 8. The positive values of $\Delta H°$ indicate an endothermic batch desulfurization process. The $\Delta S°$ positive value verifies the elevated randomness of sulfur molecules on the solid surface compared to those in the

Table 3 Comparison between this study and other studies

No.	Sample	Adsorbent	System	sulfur Content (ppm)	% Sulfur Removal	Refs.
1	Diesel fuel	Ni/MCM-41	Batch	250	58%	[42]
2	Diesel fuel	MCM-41	Batch	250	96.5%	[43]
3	Diesel fuel	Ag/MCM-41	Batch	1234.9	95.6%	[44]
4	Actual heavy crude oil	AC	Batch	18,000	28%	This study

solution [41]. The ΔG° negative values indicate that the adsorption of sulfur components of the oil after treatment happened spontaneously over the whole studied temperature range. Enthalpy change (ΔHo) insinuates that the adsorption kind is chemisorption if more than 40 kJ/mol and physisorption if less than 20 kJ/mol. Thus, it is physisorption, as demonstrated in Table 2, this is established on the way the forces of Vander Waals interact.

3.6 Optimum conditions

The best adsorption rate of sulfur components from the heavy crude oil was obtained from the three studied variables, such as; a dose of AC = 0.8 gm, contact time = 1.5 h, and temperature = 50 °C, respectively. This research reveals that the sulfur concentration can be decreased from 2.5 wt.% to 1.8 wt.%. However, adsorption desulfurization has an efficiency of approximately 28% and is effective at removing the sulfur elements. This study utilized particles with an average size of 0.8 mm AC because they are available in this size commercially. Of course, activated carbon with different particle sizes will have an effect on the results, but it is not investigated in this study. The viscosity of heavy crude oil is very high. Therefore, the small particle is not recommended because of the difficulties of filtration during separation.

3.7 Comparative study

In this work, a batch adsorption technique is used to extract sulfur compounds from actual heavy crude oil by implying AC, since AC has quite a considerable surface area of 519.4 m^2/g and is a low price material when compared to other adsorbents. Besides this, this technique has the potential to be used to remove extra sulfur compounds while treating actual fuel owing to its ability to deal with several-sided processes, which can lower operational expenses and processing. In Table 3, studies are assessed, revealing the potential of AC as an adsorbent for eliminating sulfur compounds with a removal efficiency of 28%.

4 Conclusion

Based on the results of the current experimental investigation and those of a desulfurization procedure utilized to remove sulfur from heavy crude oil, it was observed that the asorption desulfurization efficiency increased with increasing adsorption temperature, time of adsorption contact, and sorbent dose. A precise characterization of the desulfurization process has been observed through the Temkin model, which is the best isotherm match, and possesses the maximum correlation coefficient (0.974) among the studied adsorption isotherms of the treated oil. The kinetic analysis demonstrated that the pseudo-first-order kinetic model very fit and obtained the optimum match for a straight line of correlation coefficient ($R^2 = 0.955$). The thermodynamic essential parameters (ΔG°), (ΔH°), and (ΔS°) were acquired for this experiment and demonstrated that the adsorption of sulfur elements on the AC is endothermic and spontaneous, along with enhancing the distribution of sulfur compounds at random places on the surface of the adsorbent. The optimum operating conditions of 0.8 gm of AC, 1.5 h, and 50 °C contributed to the reduction of the sulfur content to 1.8 wt%. The removal of sulfur was achieved with a 28% efficiency.

Acknowledgements The authors gratefully sincerely thank the Chemical Engineering Department of the University of Technology – Iraq, due to their assistance with this study.

Funding Not Applicable.

Availability of data and material All relevant data and material are presented in the main paper.

Declarations

Conflict of interests The authors declare that they have no competing interests.

Ethics approval and consent to participate Not applicable.

Consent for publication Not applicable.

References

1. Yang C, Zhao K, Cheng Y, Zeng G, Zhang M, Shao J, Lu L (2016) Catalytic oxidative desulfurization of BT and DBT from n-octane using cyclohexanone peroxide and catalyst of molybdenum supported on 4A molecular sieve. Sep Purif Technol 163:153–161
2. Li C, Li D, Zou S, Li Z, Yin J, Wang A, Zhao Q (2013) Extraction desulfurization process of fuels with ammonium-based deep eutectic solvents. Green Chem 15(10):2793–2799
3. Fan J, Chen A, Saxena S, Vedachalam S, Dalai AK, Zhang W, Roberts WL (2021) Ultrasound-assisted oxidative desulfurization of Arabian extra light oil (AXL) with molecular characterization of the sulfur compounds. Fuel 305:121612
4. Palomino JM, Tran DT, Kareh AR, Miller CA, Gardner JM, Dong H, Oliver SR (2015) Zirconia-silica based mesoporous desulfurization adsorbents. J Power Sources 278:141–148
5. Saleh TA (2018) Simultaneous adsorptive desulfurization of diesel fuel over bimetallic nanoparticles loaded on activated carbon. J Clean Prod 172:2123–2132
6. Mohammed YM, Albayati TM, Ali AM (2022) Imidazolium-based ionic liquids for extraction of sulfur compounds from real heavy crude oil. Chem Afr. https://doi.org/10.1007/s42250-022-00447-9.
7. Takahashi A, Yang FH, Yang RT (2002) New sorbents for desulfurization by π-complexation: thiophene/benzene adsorption. Ind Eng Chem Res 41(10):2487–2496
8. Hammad AD, Yusuf Z, Al-Rasheedi N (2012) In-situ electrochemical desulfurization of crude oil and its fraction. Saudi Aram J Technol: 1–5.
9. Kalavathy H, Karthik B, Miranda LR (2010) Removal and recovery of Ni and Zn from aqueous solution using activated carbon from Hevea brasiliensis: batch and column studies. Coll Surf B 78(2):291–302
10. Yu G, Lu S, Chen H, Zhu Z (2005) Diesel fuel desulfurization with hydrogen peroxide promoted by formic acid and catalyzed by activated carbon. Carbon 43(11):2285–2294
11. Khadim AT, Albayati TM, Saady NM (2022) Removal of sulfur compounds from real diesel fuel employing the encapsulated mesoporous material adsorbent Co/MCM-41 in a fixed-bed column., Microp Mesop Mater 341: 112020. https://doi.org/10.1016/j.micromeso.2022.112020.
12. Al Zubaidi I, Darwish NN, El Sayed Y, Shareefdeen Z, Sara Z (2015) Adsorptive desulfurization of commercial diesel oil using granular activated charcoal. Int J Adv Chem Eng Biol Sci 2(1):15–18
13. Ibrahim NK, Aljanabi SK (2015) Desulfurization and kinetic study of diesel fuel by batch adsorption on activated carbon. Eng Technol J 33(8).
14. Mohammed MY, Ali AM, Albayati TM (2022) Choline chloride-based deep eutectic solvents for ultrasonic-assisted oxidative desulfurization of actual heavy crude oil. Chem Eng Res Des 182:659–666
15. Shu J, Cheng S, Xia H, Zhang L, Peng J, Li C, Zhang S (2017) Copper loaded on activated carbon as an efficient adsorbent for removal of methylene blue. RSC Adv 7(24):14395–14405
16. Olajire AA, Abidemi JJ, Lateef A, Benson NU (2017) Adsorptive desulphurization of model oil by Ag nanoparticles-modified activated carbon prepared from brewer's spent grains. J Environ Chem Eng 5(1):147–159
17. Langmuir I (1916) The constitution and fundamental properties of solids and liquids. Part I. Solids. J Am Chem Soc 38(11): 2221–2295
18. Freundlich H (1907) Über die adsorption in lösungen. Z Phys Chem 57(1):385–470
19. Al-Jaaf HJ, Ali NS, Alardhi SM, Albayati TM (2022) Implementing eggplant peels as an efficient bio-adsorbent for treatment of oily domestic wastewater. Desalin Water Treat 245:226–237
20. Khader EH, Mohammed TJ, Albayati TM (2021) Comparative performance between rice husk and granular activated carbon for the removal of azo tartrazine dye from aqueous solution. Desalin Water Treat 229:372–383
21. Khadim AT, Albayati TM, Saady NMC (2022) Desulfurization of actual diesel fuel onto modified mesoporous material Co/MCM-41. Environ Nanotechnol Monit Manag 17:100635
22. Temkin M, Pyzhev V) 1940(Kinetics of the synthesis of ammonia on promoted iron catalysts. J Phys Chem (USSR) 13: 851–867
23. Alardhi SM, Alrubaye JM, Albayati TM (2020) Removal of methyl green dye from simulated waste water using hollow fiber ultrafiltration membrane. In: IOP Conference Series: Materials Science and Engineering (Vol. 928, No. 5, p. 052020). IOP Publishing.
24. Kadhum ST, Alkindi GY, Albayati TM, Treatment W (2021) Determination of chemical oxygen demand for phenolic compounds from oil refinery wastewater implementing different methods. Desalin Water Treat 231:44–53
25. Ali NS, Jabbar NM, Alardhi SM, Majdi HS, Albayati TM (2022) Adsorption of methyl violet dye onto a prepared bio-adsorbent from date seeds: isotherm, kinetics, and thermodynamic studies. Heliyon: e10276.
26. Jha D, Haider MB, Kumar R, Byamba-Ochir N, Shim WG, Marriyappan Sivagnanam B, Moon H (2019) Enhanced adsorptive desulfurization using Mongolian anthracite-based activated carbon. ACS Omega 4(24):20844–20853
27. Muslim WA, Albayati TM, Al-Nasri SK (2022) Decontamination of actual radioactive wastewater containing 137Cs using bentonite as a natural adsorbent: equilibrium, kinetics, and thermodynamic studies. Sci Rep 12(1):1–12
28. Kadhum ST, Alkindi GY, Albayati TM (2022) Remediation of phenolic wastewater implementing nano zerovalent iron as a granular third electrode in an electrochemical reactor. Int J Environ Sci Technol 19(3):1383–1392
29. Nurul'ain BJ (2007) The production and characterization of activated carbon using local agricultural waste through chemical activation process. Int J Environ Bioenergy Res Gate: 1–24.
30. Lee SM, Lee SH, Roh JS (2021) Analysis of activation process of carbon black based on structural parameters obtained by XRD analysis. Curr Comput Aided Drug Des 11(2):153
31. Ovchinnikov OV, Evtukhova AV, Kondratenko TS, Smirnov MS, Khokhlov VY, Erina OV (2016) Manifestation of intermolecular interactions in FTIR spectra of methylene blue molecules. Vib Spectrosc 86:181–189
32. Houda S, Lancelot C, Blanchard P, Poinel L, Lamonier C (2018) Oxidative desulfurization of heavy oils with high sulfur content: a review. Catalysts 8(9):344
33. Tetrisyanda R, Wiguno A, Ginting RR, Dzikrillah MC, Wibawa G (2017) Residue oil desulfurization using oxidation and extraction method. Indonesian J Chem 18(2):242–249
34. Vijayaraghavan K, Padmesh TVN, Palanivelu K, Velan M (2006) Biosorption of nickel (II) ions onto Sargassum wightii: application of two-parameter and three-parameter isotherm models. J Hazard Mater 133(1–3):304–308
35. Saleh TA, Sulaiman KO, Al-Hammadi SA, Dafalla H, Danmaliki GI (2017) Adsorptive desulfurization of thiophene, benzothiophene and dibenzothiophene over activated carbon manganese oxide nanocomposite: with column system evaluation. J Clean Prod 154:401–412
36. Lagergren S (1898) Zur theorie der sogenannten adsorption geloster stoffe. Kungliga Svenska Vetenskapsakademiens Handlingar 24:1–39

37. Nkosi M (2014) Desulphurisation of petroleum distillates using adsorption method (Doctoral dissertation, University of the Witwatersrand, Faculty of Engineering and the Built Environment, School of Chemical and Metallurgical Engineering).
38. Rezvani MA, Miri OF (2019) Synthesis and characterization of PWMn/NiO/PAN nanosphere composite with superior catalytic activity for oxidative desulfurization of real fuel. Chem Eng J 369:775–783
39. Rezvani MA, Rahmani P (2019) Synthesis and characterization of new nanosphere hybrid nanocomposite polyoxometalate@ ceramic@ polyaniline as a heterogeneous catalyst for oxidative desulfurization of real fuel. Adv Powder Technol 30(12):3214–3223
40. Weber TW, Chakravorti RK (1974) Pore and solid diffusion models for fixed-bed adsorbers. AIChE J 20(2):228–238
41. Tan IAW, Ahmad AL, Hameed BH (2009) Adsorption isotherms, kinetics, thermodynamics and desorption studies of 2, 4, 6-trichlorophenol on oil palm empty fruit bunch-based activated carbon. J Hazard Mater 164(2–3):473–482
42. García-Martínez JC, González-Uribe HA, González-Brambila MM, del Río NG, López-Gaona A, Alvarado-Perea L, Colín-Luna JA (2018) Effect of Ni on MCM-41 in the adsorption of nitrogen and sulfur compounds to obtain ultra-low-sulfur diesel. Top Catal 61(15):1721–1733
43. Sadare OO, Masitha IM, Daramola MO (2021) Synthesis, characterization and performance evaluation of pure silica MCM-41 for effective removal of dibenzothiophene from petroleum distillate. In IOP Conference Series: Materials Science and Engineering (Vol. 1107, No. 1, p. 012041). IOP Publishing.
44. Sales VR, Moura HO, Câmara AB, Rodríguez-Castellón E, Silva JA, Pergher SB, de Carvalho LS (2019) Assessment of Ag nanoparticles interaction over low-cost mesoporous silica in deep desulfurization of diesel. Catalysts 9(8):651